STUDYING EFFECTS OF FINS AND CONDUCTIVE HORIZONTAL WALLS ON NATURAL CONVECTION IN DIFFERENTIALLY HEATED ENCLOSURES

Elin Vesper[1,2], Sebastian Tietjen[1], Manu Chakkingal[1,2], Saša Kenjereš[1,2*]

[1]Transport Phenomena Section, Chemical Engineering Department, Faculty of Applied Sciences, Delft University of Technology, Van der Maasweg 9, 2629 HZ Delft, The Netherlands
[2]J.M. Burgerscentrum Research School for Fluid Mechanics, Mekelweg 2, 2628 CD Delft, The Netherlands

ABSTRACT

In the present study, we addressed the influence of the horizontal conducting walls and a heated fin on the flow, turbulence, and heat transfer inside the side-heated air-filled enclosure over a range of Rayleigh numbers ($10^4 \leq Ra \leq 10^9$) – in both 2D and 3D simulation domains. We apply a fully resolving (DNS) for a lower range of *Ra* and well-resolving (LES) numerical simulations for higher *Ra* range. For the latter, a dynamic approach is used for the calculation of the sub-grid turbulent heat flux. The simulations revealed a very good agreement of the integral heat transfer at the side cold wall between 2D and 3D approaches for the empty/smooth enclosure with both adiabatic- and conducting-horizontal walls. The presence of the fin significantly affected local flow and heat transfer distributions. At Ra=10^9, the fin configuration produced enhancement of the integral heat transfer at the cold wall of 18% and 21% for adiabatic- and conducting-horizontal walls, respectively. In contrast to the integral heat transfer, the local distribution of Nusselt numbers along the fin was significantly underpredicted by 2D simulations (up to 50%).

1. INTRODUCTION AND CONSIDERED SETUP(S)

Natural convection in differentially heated cavities represents fundamental heat transfer phenomena occurring in numerical technological applications such as: solar collectors, refrigerators, passive safety systems in nuclear power plants, indoor climate, etc. The onset of turbulence may be crucial for heat transfer enhancement in these applications, [1]. The standard 'empty' differentially heated cavities filled with working fluid with adiabatic horizontal walls are extensively studied in the literature. In contrast to this case, the effects of fins and horizontally conductive walls, which are both are common in real industrial and technological applications, are much less investigated. To fill this gap in the studies of the natural convection, and to provide detailed information on local and integral flow and heat transfer features, we generate and numerically simulate four setups: (i) empty/smooth cavity with adiabatic horizontal walls (SC-AHW), (ii) empty/smooth cavity with perfectly conductive horizontal walls (SC-CHW) (note that here we introduce a definition of the 'smooth cavity' indicating configuration without obstacles/fins), (iii) cavity with a fin and adiabatic horizontal walls (FC-AHW), and, (iv) cavity with a fin and perfectly conducting horizontal walls (FC-CHW), as shown in Figs.1(a-d) and Table 1. All setups are simulated in both 2D (square enclosure) and 3D (cubical enclosure with periodic boundary conditions in the span-wise z-direction) domains. We select air as a working fluid (with constant thermophysical properties), with *Pr*=0.71, and apply the Boussinesq approximation in the momentum equation.

2. TURBULENCE CLOSURE AND NUMERICAL MESH

Numerical simulations are conducted over an extensive range of Rayleigh numbers, i.e. $10^4 \leq Ra \leq 10^9$ where Direct Numerical Simulation (DNS) is applied in the lower range ($10^4 \leq Ra \leq 10^7$) and wall-

*Corresponding Author: s.kenjeres@tudelft.nl

resolving Large Eddy Simulation (LES) in the upper range ($10^8 \leq Ra \leq 10^9$). For the latter one, we use the WALE sub-grid closure for the momentum, [2], and the dynamic eddy diffusivity sub-grid model for the temperature equation, [3]. The letter is selected since it does not require *a priory* specification of the turbulent Prandtl number since it will be directly evaluated from the dynamic procedure. Special attention is devoted to a proper numerical resolving of the thermally active near-wall regions. Details of the applied numerical mesh with a characteristic number of control volumes used to resolve thermal boundary layers are provided in Table 2. To confirm the adequacy of the applied numerical resolution, we plot contours of the ratio of the long-term time-averaged sub-grid turbulent and molecular viscosity, as well as of the sub-grid and total turbulent kinetic energy in the central vertical plane, for the highest simulated value of $Ra=10^9$ and perfectly thermally conducting horizontal walls, Figs.1.(e,f).

3. INSTANTANEOUS TEMPERATURE AND FLOW FIELD

The instantaneous temperature fields in the central vertical plane are shown in Fig.2. For lower value or $Ra=10^7$, for the empty/smooth configurations – with adiabatic horizontal walls – the flow is still in a laminar flow regime, Fig.2(a). The flow instabilities start to appear after imposing the conducting horizontal walls or by inserting the heated fin. For the former, a local acceleration of the horizontal jet generates additional momentum along the heated/cooled vertical walls, respectively. For the latter, the presence of the fin imposes the lower (stable stratified) and upper (unstable stratified) compartments. For the upper compartment, we have a combination of the Rayleigh-Benard-like (heated from the upper surface of the fin) and side-heated wall-jet instabilities, Figs.2(b,c,d). At a higher value of $Ra=10^9$, thinner boundary layers along the vertical sidewalls are generated, and a fully developed turbulent regime is obtained even for the adiabatic horizontal boundary layers situation, Figs. 2(e,f). The presence of fin generates additional thermal plumes at its top surface, producing an intensive mixing in the upper part of the enclosure, Figs.2(g,h). The horizontal conducting walls in the presence of the fin, lead to a partial reduction or a total breakdown of the stable thermally stratified regions, causing a stronger mixing also in the lower part of the enclosure, Figs.2(d,h). To illustrate full 3D flow features, we extract and visualize the instantaneous coherent structures based on the analysis of the second-invariant of the velocity gradient tensor (so-called Q-parameter, [4,5]), as shown in Fig.3. It can be seen the coherent structures are much finer for the higher value of Rayleigh number ($Ra=10^9$). Furthermore, for the empty/smooth enclosure with adiabatic horizontal walls and without the fin, the locally turbulent pockets are generated along the upper/lower parts of the thermally active side-wall, Fig.3(e). By replacing the adiabatic with conducting walls, the coherent structures cover the entire surface of the sidewalls, confirming turbulence enhancement, Fig.3(f). The introduction of the fin imposes a significant flow and turbulence reorganization. For the case with the fin and adiabatic horizontal walls, the coherent structures are now present above the fin, whereas are reduced along the cooled vertical wall, Fig.3(g). Again, the combination of the fin and conducting horizontal walls generates more dense coherent structures, Fig.3(h).

4. LOCAL HEAT TRANSFER ALONG THE FIN UPPER/LOWER SURFACES

Next, we focus on an analysis of the local heat transfer (local Nusselt number) along the upper/lower surface of the fin, since this configuration produced significant reorganization of the flow and turbulence compared to the corresponding empty enclosure, Fig.4. The profile of the instantaneous 3D local Nusselt number at the upper surface exhibits highly non-uniform behavior for both – adiabatic and conducting horizontal walls - caused by the generation of the thermal plumes. By comparing the averaged local Nusselt numbers, it can be seen that significant differences are obtained between the 3D and 2D simulations – for both adiabatic- and conducting-horizontal walls configurations, Figs.4(a),(b). The 2D simulations are producing values of approximately 50% of 3D simulations. The variation of the local Nusselt number along the lower fin surface shows much less intermittent behavior. Here, the differences between 2D and 3D simulations are significantly smaller in comparison to the upper surface.

5. INTEGRAL HEAT TRANSFER

Finally, we analyze the integral (i.e. time- and surface-averaged) Nusselt number at the cold vertical wall for all considered cases, Fig.5. We also add the lines to indicate characteristic *Nu-Ra* slopes of the power-law exponents (1/4) – for the laminar heat transfer, and (1/3) – for the turbulent heat transfer. It can be seen that a good agreement with the results from the literature is obtained for the empty/smooth configuration, [6-9]. We find that the conductive horizontal walls reduce the integral heat transfer in comparison to the adiabatic horizontal walls. For the $Ra=10^4$ case, the Nusselt number for the fin case is lower than for the empty/smooth configuration. This is caused by a flow reduction caused by the obstacle/fin. In contrast, at the high value of the Rayleigh number, i.e. $Ra=10^9$, the configuration with the fin exhibits heat transfer enhancements of 18% and 21% in comparison with the empty/smooth geometry for adiabatic- and conducting-horizontal walls, respectively. For the empty/smooth enclosure predicted integral heat transfer shows a remarkable good agreement between the 2D and 3D simulations over the entire range of Ra numbers. The differences between 2D and 3D simulations are significant for the configuration with the fin and $Ra>10^7$.

6. CONCLUSION

We find that conducting horizontal walls reduce the heat transfer at the vertical cooled side-wall in comparison to the adiabatic horizontal walls for all considered cases. At a high value of $Ra=10^9$, the presence of the fin enhances the integral heat transfer at the vertical cold wall in comparison with the empty/smooth configuration for both adiabatic- and conducting-horizontal walls. The comparison between predicted integral Nusselt numbers from 2D and 3D simulations of empty/smooth configuration revealed remarkable good agreement, independently from the type of applied boundary conditions of the horizontal walls. For the heated fin configuration, differences between 2D and 3D simulations are significant for higher values of *Ra*. In contrast to the integral heat transfer, the local heat transfer in the proximity of the fin shows significant underprediction for the 2D simulations.

REFERENCES

[1] K. Hanjalic, S. Kenjeres, F. Durst, Natural convection in partitioned two-dimensional enclosures at higher Rayleigh numbers, *Int. J. Heat Mass Transfer,* **39** (7) (1996) 1407–1427.

[2] F. Nicoud, F. Ducros, Subgrid-scale stress modeling based on the square of the velocity gradient tensor. *Flow, Turbulence and Combustion,* **62** (3) (1999) 183-200.

[3] P. Moin, K. Squires, W. Cabot, S. Lee, A dynamic subgrid-scale model for compressible turbulence and scalar transport. *Physics of Fluids A: Fluid Dynamics,* **3** (11) (1991) 2746-2757.

[4] J.C.R. Hunt, A. Wray, P. Moin, Eddies, stream, and convergence zones in turbulent flows. *Center for Turbulence Research Report CTR-S88*, (1988) 193-208.

[5] S. Kenjeres, K. Hanjalic, Identification and visualization of coherent structures in Rayleigh-Benard convection with a time-dependent RANS, *Journal of Visualization,* **2** (2) (1999) 169-176.

[6] A. Xu, L. Shi, T.S. Zhao, Accelerated lattice Boltzmann simulation using GPU and openACC with data management, *Int. J. Heat Mass Transfer,* **109** (2017) 577–588.

[7] A. Xu, L. Shi, H.-D. Xi, Lattice Boltzmann simulations of three-dimensional thermal convective flows at high Rayleigh number, *Int. J. Heat Mass Transfer,* **140** (2019) 359–370.

[8] P. Le Quéré, M. Behnia, From onset of unsteadiness to chaos in a differentially heated square cavity. *Journal of Fluid Mechanics,* **359** (1998) 81-107.

[9] F. Sebilleau, R. Issa, S. Lardeau, S.P. Walker, Direct Numerical Simulation of an air-filled differentially heated square cavity with Rayleigh numbers up to 10^{11}. *Int. J. Heat Mass Transfer,* **123** (2018) 297-319.

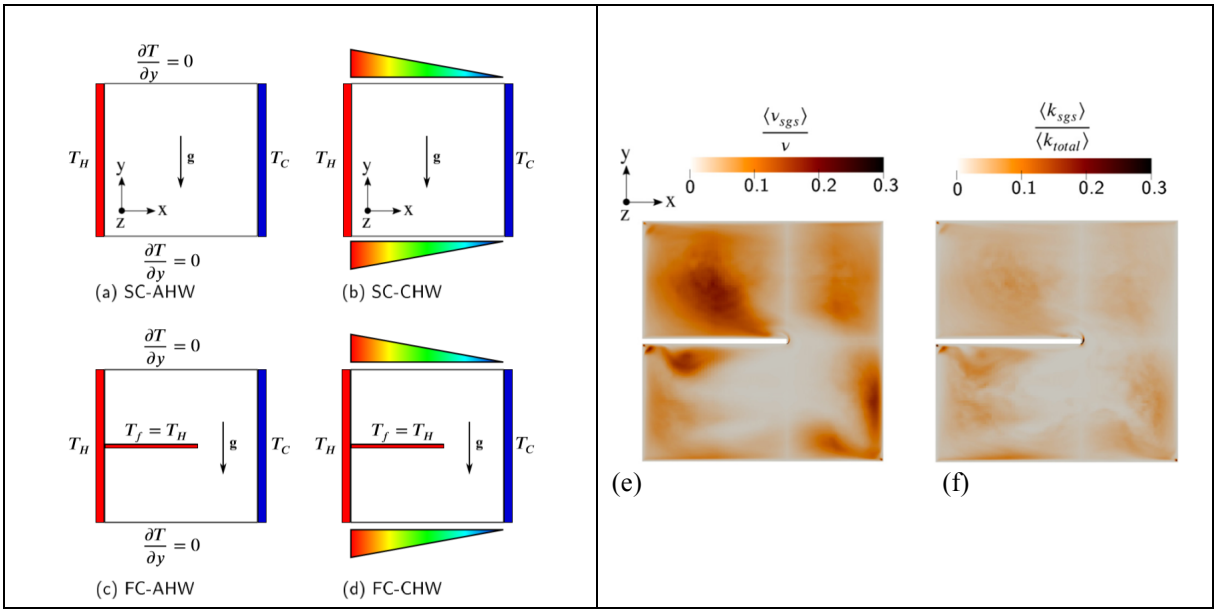

Figure 1: Sketches of the considered differentially side-heated cases for smooth and enclosures without and with fin with adiabatic and perfectly conducting horizontal walls (a-d); Contours of the long-term time-averaged ratio of the sub-grid/turbulent and molecular viscosity (e) and sub-grid and total turbulent kinetic energy (f) in the central vertical plane for the LES at Ra=10^9 case with conducting horizontal walls.

Table 1: Overview of all considered simulations with applied turbulence modeling approach (DNS or LES) and types of the horizontal walls boundary conditions.

Ra	Modeling	Case	Horizontal boundary conditions
$10^4 - 10^7$	DNS (2D/3D)	Smooth	Adiabatic
			Conductive
$10^4 - 10^7$	DNS (2D/3D)	Fin	Adiabatic
			Conductive
$10^8 - 10^9$	DNS (2D)	Smooth	Adiabatic
			Conductive
$10^8 - 10^9$	DNS (2D)	Fin	Adiabatic
			Conductive
$10^8 - 10^9$	LES (3D)	Smooth	Adiabatic
			Conductive
$10^8 - 10^9$	LES (3D)	Fin	Adiabatic
			Conductive

Table 2: Overview of all considered simulations and setups with details of the applied numerical mesh: the total number of the control volumes (cells) and their number within the boundary layers.

Simulation	Dimensions	Rayleigh	Smooth case		Fin case		Cells
Type	*LxHxW* [m]	number	Cells [*M*]	Cells *XxYxZ*	Cells [*M*]	Cells *XxYxZ*	in BL
	$1 \times 1 \times 1$	10^4	0.6	$76 \times 100 \times 76$	0.5	$75 \times 98 \times 75$	14
	$1 \times 1 \times 1$	10^5	0.6	$76 \times 100 \times 76$	0.5	$75 \times 98 \times 75$	8
DNS	$1 \times 1 \times 1$	10^6	0.6	$76 \times 100 \times 76$	0.5	$75 \times 98 \times 75$	4
	$1 \times 1 \times 1$	10^7	2.7	$164 \times 164 \times 100$	2.7	$164 \times 164 \times 100$	6
	$1 \times 1 \times 1$	10^8	1.2	$110 \times 110 \times 110$	2.5	$166 \times 178 \times 83$	7
LES	$1 \times 1 \times 0.5$	10^9	1.8	$154 \times 154 \times 77$	3.3	$246 \times 256 \times 55$	9

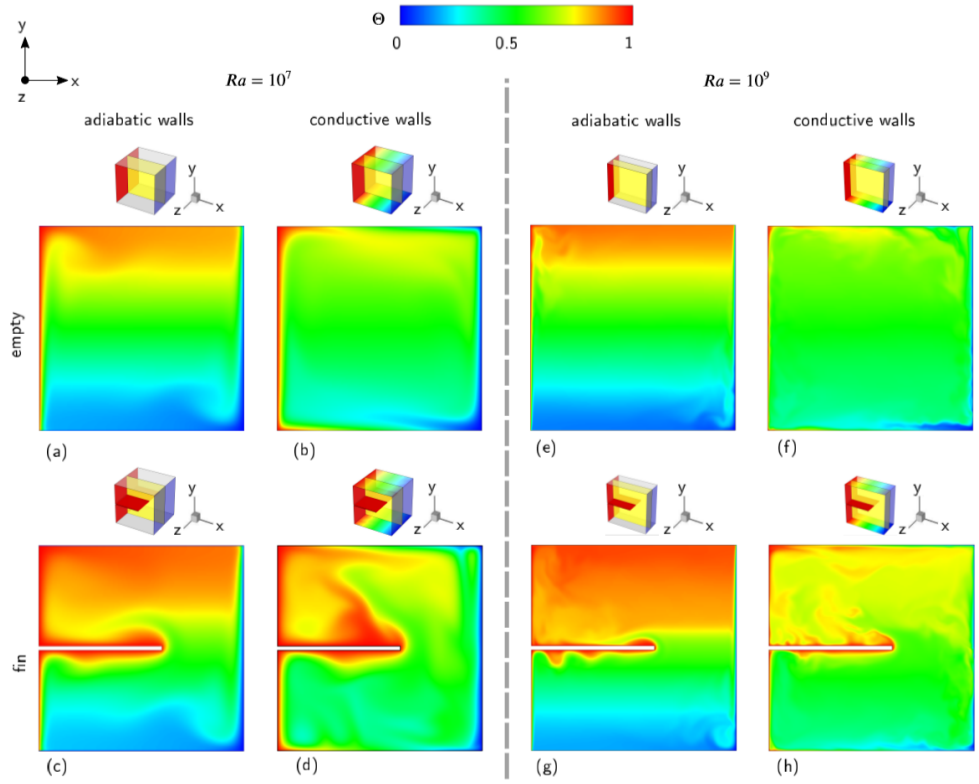

Figure 2: Instantaneous normalised temperature field for (a)-(d) Ra=10^7 and (e)-(f) Ra=10^9.

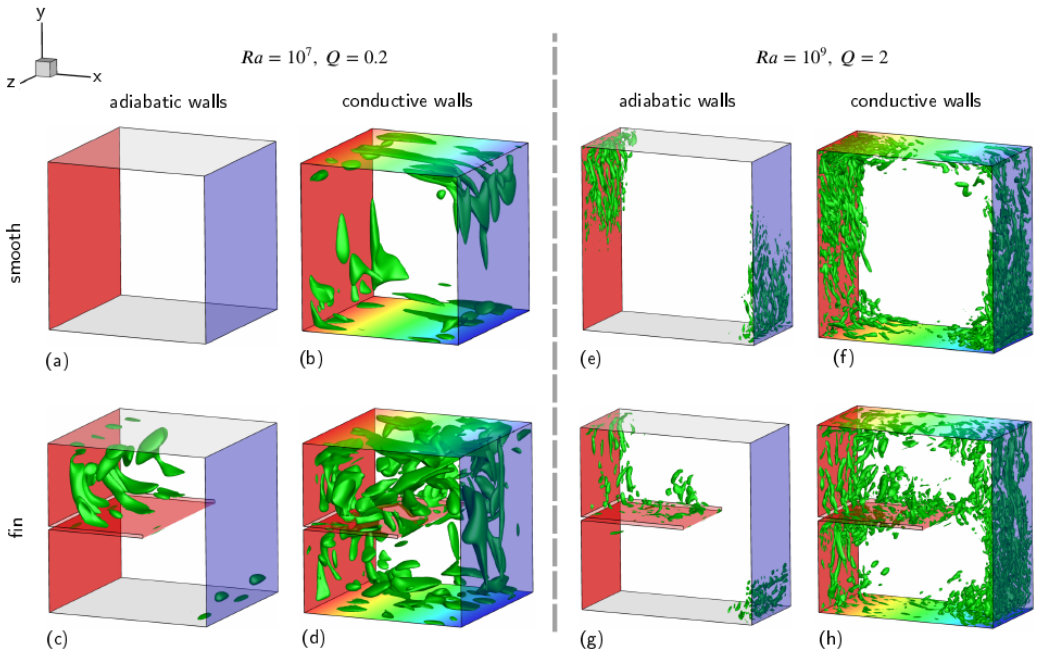

Figure 3: Iso-surfaces of the instantaneous Q-parameter: (a)-(d) at Ra=10^7 for Q=0.2 $1/s^2$ and (e)-(h) at Ra=10^9 for Q=2 $1/s^2$.

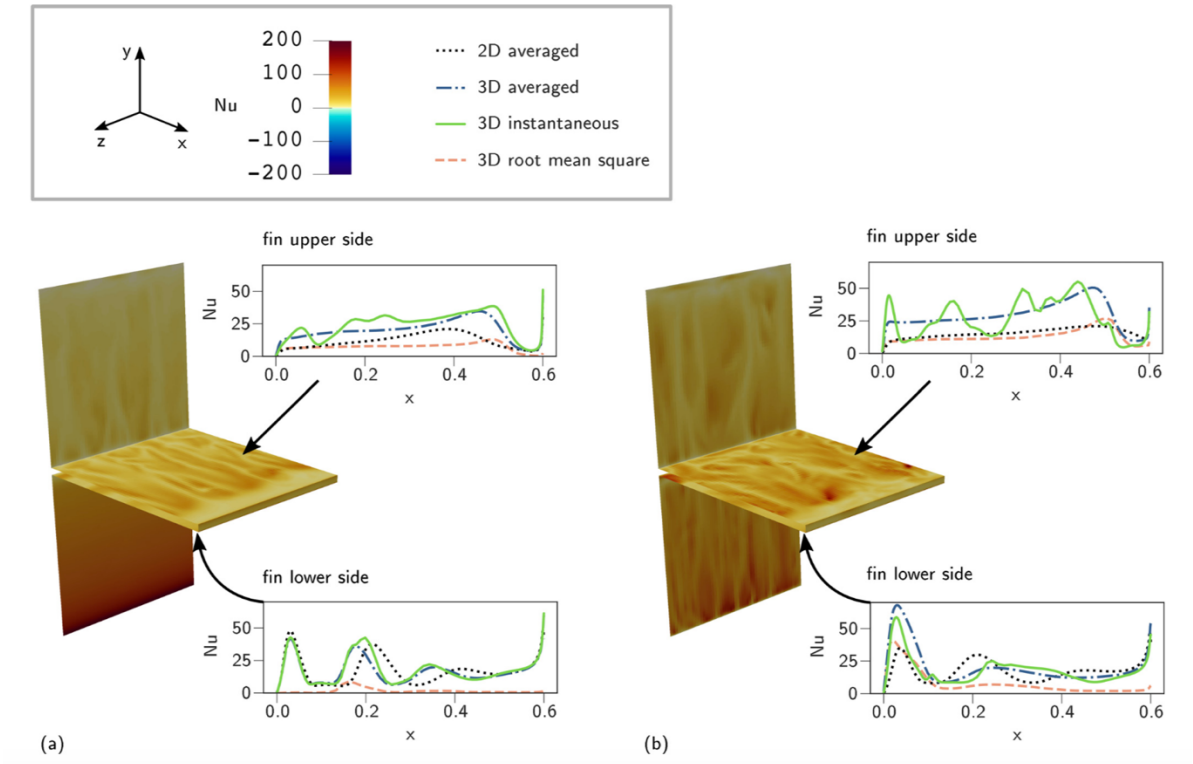

Figure 4: The local Nusselt number plots (2D-averaged, 3D-averaged, 3D-instantaneous, 3D- RMS) for the upper and lower side of the fin: (a) adiabatic horizontal walls and (b) conductive horizontal walls at Ra=10^9 (LES results).

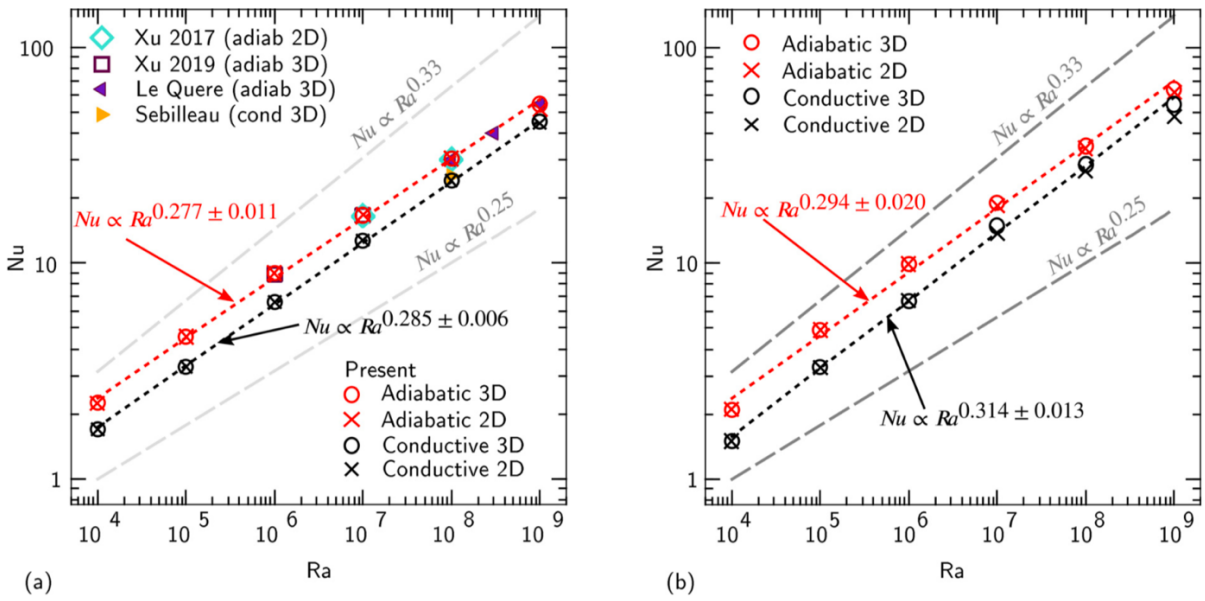

Figure 5: The Nusselt-Rayleigh dependency at the cold wall for the smooth/empty cavity (a) and the cavity with the fin (b) for 2D and 3D simulations. The dashed grey lines denote the laminar (the power-law exponent of 1/4) and turbulent (the power-law exponent of 1/3) slopes. The smooth cases (the empty enclosure) are compared with data by Xu et al. [6,7], Le Quéré, and Behnia [8] for adiabatic horizontal walls and Sebilleau et al. [9] for conductive horizontal walls.